

Characterization of diamond-like nanocomposite thin films grown by plasma enhanced chemical vapor deposition

T. S. Santra, C. H. Liu, T. K. Bhattacharyya, P. Patel, and T. K. Barik

Citation: [Journal of Applied Physics](#) **107**, 124320 (2010); doi: 10.1063/1.3415548

View online: <http://dx.doi.org/10.1063/1.3415548>

View Table of Contents: <http://scitation.aip.org/content/aip/journal/jap/107/12?ver=pdfcov>

Published by the [AIP Publishing](#)

Articles you may be interested in

[Influence of flow rate on different properties of diamond-like nanocomposite thin films grown by PECVD](#)
AIP Advances **2**, 022132 (2012); 10.1063/1.4721654

[The study on the effect of erbium on diamond-like carbon deposited by pulsed laser deposition technique](#)
J. Appl. Phys. **106**, 064904 (2009); 10.1063/1.3211986

[Synthesis of tin-incorporated nanocomposite diamond like carbon films by plasma enhanced chemical vapor deposition and their characterization](#)
J. Vac. Sci. Technol. B **22**, 2709 (2004); 10.1116/1.1815318

[Structural and mechanical properties of diamond-like carbon films deposited by direct current magnetron sputtering](#)
J. Vac. Sci. Technol. A **21**, 851 (2003); 10.1116/1.1575231

[Diamond-like carbon nanocomposite films](#)
Appl. Phys. Lett. **82**, 3526 (2003); 10.1063/1.1576909



AIP | Journal of Applied Physics

Journal of Applied Physics is pleased to announce **André Anders** as its new Editor-in-Chief

Characterization of diamond-like nanocomposite thin films grown by plasma enhanced chemical vapor deposition

T. S. Santra,¹ C. H. Liu,¹ T. K. Bhattacharyya,² P. Patel,³ and T. K. Barik^{4,a)}

¹*Institute of Nanoengineering and Microsystems (NEMS), National Tsing Hua University, Hsinchu, Taiwan 30043, Republic of China*

²*Department of Electronics and Electrical Communication Engineering, Indian Institute of Technology, Kharagpur 721302, West Bengal, India*

³*Department of Electrical and Computer Engineering, University of Illinois at Urbana Champaign, Urbana, Illinois 61801, USA*

⁴*School of Applied Sciences, Haldia Institute of Technology, Haldia 721657, Purba Medinipur, West Bengal, India*

(Received 22 December 2009; accepted 3 April 2010; published online 25 June 2010)

Diamond-like nanocomposite (DLN) thin films, comprising the networks of a-C:H and a-Si:O were deposited on pyrex glass or silicon substrate using gas precursors (e.g., hexamethyldisilane, hexamethyldisiloxane, hexamethyldisilazane, or their different combinations) mixed with argon gas, by plasma enhanced chemical vapor deposition technique. Surface morphology of DLN films was analyzed by atomic force microscopy. High-resolution transmission electron microscopic result shows that the films contain nanoparticles within the amorphous structure. Fourier transform infrared spectroscopy (FTIR), Raman spectroscopy, and x-ray photoelectron spectroscopy (XPS) were used to determine the structural change within the DLN films. The hardness and friction coefficient of the films were measured by nanoindentation and scratch test techniques, respectively. FTIR and XPS studies show the presence of C—C, C—H, Si—C, and Si—H bonds in the a-C:H and a-Si:O networks. Using Raman spectroscopy, we also found that the hardness of the DLN films varies with the intensity ratio I_D/I_G . Finally, we observed that the DLN films has a better performance compared to DLC, when it comes to properties like high hardness, high modulus of elasticity, low surface roughness and low friction coefficient. These characteristics are the critical components in microelectromechanical systems (MEMS) and emerging nanoelectromechanical systems (NEMS). © 2010 American Institute of Physics. [doi:10.1063/1.3415548]

I. INTRODUCTION

Diamond-like carbon (DLC) or amorphous carbon has generated a great interest in the academia due to its fundamental and technological importance. DLC films have excellent properties, like high hardness, very low friction coefficient, wear chemical inertness, low surface roughness, and optical transparency in the infrared range. These films are currently used as a wear resistant coating for hard-disk drive, optical component, or in the form of biocompatible coatings for medical purpose.^{1–7} DLC films have some disadvantages, like they cannot withstand their particular characteristics at a higher temperature because of the conversion of sp^3 hybridized carbon to sp^2 hybridized carbon. Siegal *et al.*^{8,9} reported that the high compressive stress (~ 6 – 12 GPa) of the amorphous tetrahedral DLC film which is deposited at room temperature, can be relieved by postannealing at 600 °C. Moreover, the intrinsic compressive stress between the films and substrate of the DLC films is very high. Usually, this provides the poor adhesion between films and substrate. In order to reduce the stress of the films, much attention has recently been paid to controlling the nanostructure of the DLC films, without leaving its hardness.^{10–13}

In order to overcome these disadvantages of DLC films, we recommend the use of Diamond-like nanocomposite

(DLN) thin films. These films consist of carbon network mainly in the form of diamond-like bonds (sp^3), which are chemically stabilized by hydrogen atoms and quartzlike silicon network which are chemically stabilized by oxygen atoms resulting in a pure amorphous structure.¹⁴ Moreover, atomic or molecular dopantlike transition metals, ceramic compounds can be introduced as third random network into the films to improve the electrical, mechanical, and thermal properties. DLN films usually consist of a mixture of sp^2 (threefold) and sp^3 (fourfold) bonds. Properties of the DLN films can be determined by the ratio of $sp^3:sp^2$ hybridized carbon. High hardness of DLN films can be attributed to the tetrahedral coordinate with sp^3 hybridized C—C bonding network. The stress generated in the films is also associated with the concentration of sp^3 -sites created during the films growth.^{15,16} DLN films also have many applications which include low friction coatings, anti-wear, corrosion and erosion-resistant coatings, abrasion-resistant coatings for IR windows and biocompatible coatings.¹⁷ However, DLN films have a significant advantage over conventional DLC films in both stability and ability to tailor specific properties over a wide range.

II. EXPERIMENTAL DETAILS

A. Preparation of DLN films

DLN thin films were deposited on pyrex glass or silicon substrate by plasma enhanced chemical vapor deposition

^{a)}Author to whom correspondence should be addressed. Electronic mail: tarun.barik2003@gmail.com.

TABLE I. Experimental parameters for the deposition of DLN films by PECVD technique.

Precursors used in DLN films	Deposition time (h)	rf bias (V)
(a) HMDS	1	600
(b)HMDSO	1	600
(c) 50% HMDSO+50% HMDSN	1	600
(d) HMDSN	1	600

(PECVD) technique using gas precursors like hexamethyldisilane (HMDS), hexamethyldisiloxane (HMDSO), hexamethyldisilazane (HMDSN), or different combinations of the above precursors. At first, the substrate (pyrex glass or silicon) was cleaned by ultrasonic bath using acetone as well as warm trichloroethylene for five minutes and was dried by using nitrogen gas for removing the water molecule from the surface. Afterwards, the substrate was cleaned by methanol in ultrasonic bath for ten minutes. Then the substrate was rinsed in deionized water for two to three minutes and was again dried by nitrogen gas. Further, the substrate was cleaned *in situ* by argon-plasma etching, prior to deposition (here argon as the gas source in vaporization chamber). The gas precursors like HMDS, HMDSO, HMDSN, or (50% HMDSO+50% HMDSN) was dispensed in the plasma chamber. The amount of gas precursors (HMDS, HMDSO, or HMDSN) influences the property and composition of the films. We have used dc as well as rf bias as stated below for deposition of the films. Due to hot filament, the gas precursors or their combinations are ionized; as a result, the dc discharge plasma was produced. Substrate temperature was kept around 250 °C by flowing cold water through the substrate holder assembly. In order to ensure the uniform thickness of the films, the arrangement of the vaporization chamber was maintained to provide a planetary motion to the substrate holder plate. The growth rate was maintained at 1 $\mu\text{m}/\text{hour}$. The deposition parameters were maintained as follows:

- (1) chamber pressure during film growth $\approx 4 \times 10^{-4}$ Torr,
- (2) substrate holder potential ≈ 500 V, and
- (3) rf power $\approx 2 \times 10^3$ W m^{-2} .

In this deposition, variation in the ratio of precursors alters the carbon and silicon ratio in the films. Different types of precursors used in deposition, deposition time, and rf bias voltages for different samples are given below in Table I.

B. Characterization of DLN films

Nanoparticles on DLN films were analyzed using high-resolution transmission electron microscope, HRTEM (C M 12, PHILIPS TEM) along with energy dispersive x-ray (EDX) analyzer attachment. The structure and different types of bonds present in the DLN films were determined by Fourier transform infrared spectroscopy (FTIR, Nexus 870) within the wave number region 500–4000 cm^{-1} . Also, the evaluation of the material properties of the deposited films within the wave number range 400–2000 cm^{-1} , was done using Raman spectroscopy (Ranishaw, LRM-1000B). An

argon-ion laser source of power 50 mW, having wavelength of 514.5 nm was used for this study. The Raman parameters like peak position, full width at half maximum (FWHM), and intensity ratio (I_D/I_G) of D and G peaks of the DLN films were estimated by using Gaussian deconvolution the Raman spectra.¹⁸ X-ray photoelectron spectroscopy (XPS) was carried out using ESCALAB MKII Spectrometer (VG scientific, U.K.). Al K_{α} (~ 1486.6 eV) was used as an incident X-ray source, operating with pass energy ~ 50 eV for analysis of the energy of photoelectrons, which provides an overall spectral resolution ~ 1 eV for photoelectron peaks. The grading incidence x-ray diffraction (GIXRD), FTIR, Raman spectroscopy, and XPS results conform to a large extent with structural models.^{19,20} An atomic force microscope (AFM, Nanoscope E, Digital Instrument, USA) was used to observe the surface morphology, and in contact mode it was used to obtain the surface roughness of DLN films.

C. Mechanical properties

Hardness and modulus of elasticity of the deposited films was measured using nanoindentation XP (MTS, System Corporation). For nanohardness and elastic modulus measurements, the indentation tests were performed under an applied load of 20 mN using Berkovich-type diamond tip (3-sided pyramidal indenter). The total included angle of this tip was 142.3 degree, with a half angle of 65.35 degree. The diameter of the tip was around 100 nm. The holding time for each indentation was 5 s. The rate of approach of the indenter to the surface was 25 nm/s. The maximum indentation into the surface was 300 nm. The nanohardness and modulus of elasticity was determined by the Oliver and Pharr method.²¹ Friction coefficient of the films was measured by scratch tester (TR 101, Ducom) under the load of 16 N with a loading rate 5 N/mm. The scratch length was set to at 3 mm. The normal force was divided by lateral force to estimate the coefficient of friction of the DLN films.

III. RESULTS

A. Characterization of nanocomposite films

In this article, the experimental results of four types of DLN samples deposited on pyrex glass or silicon substrate using the gas precursors like HMDS, HMDSO, HMDSN, or 50% HMDSO+50% HMDSN are discussed. Actually, the silicon substrate was only used to perform the HRTEM and AFM measurements (due to experimental advantage) and the pyrex glass substrate was used in all other characterizations. However, in near future, we have a plan to study the effects due to substrate variation in DLN films by using different characterization techniques.

The GIXRD spectrum of DLN films (for HMDS precursor) deposited on pyrex glass substrate has been shown in Fig. 1. In this figure, there is no sharp peak or big hump with detectable crystallinity. Hence, we can conclude that the undoped DLN films are amorphous in nature.

The HRTEM image in Fig. 2 of DLN films (for HMDSN precursor) on silicon substrate confirm the nucleation and growth of Si_3N_4 nanoparticles in the amorphous matrix of sizes 6–30 nm. On the other hand, SiC and SiO_x nanopar-

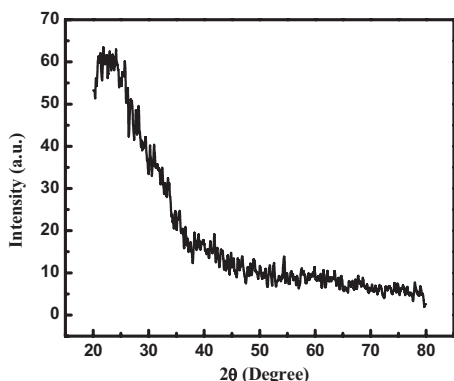
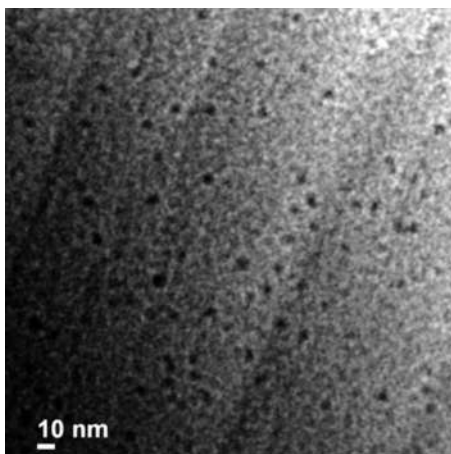


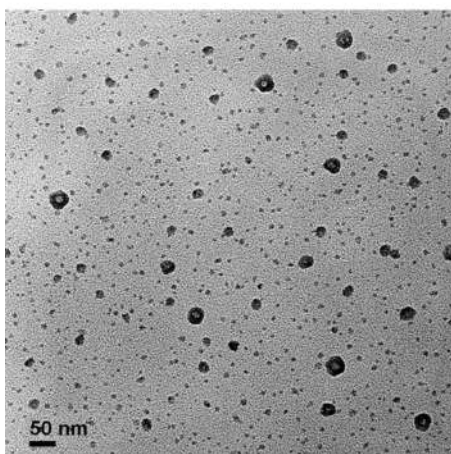
FIG. 1. The GIXRD spectrum of DLN films (for HMDS precursor) deposited on pyrex glass substrate.

ticles having same sizes were found in the DLN films using HMDS and HMDSO precursors, respectively.

The FTIR spectroscopy is a standard method for investigating the bond structure of atoms by using the IR absorption spectrum.²² The FTIR spectra of DLN films for four different types of precursors are shown in Fig. 3. From FTIR spectra, it is found that DLN films predominantly consist of C—C, C—H, Si—C, and Si—H bonds. In these four types of DLN films (mentioned above), a narrow absorption band



(a)



(b)

FIG. 2. HRTEM image of DLN films on silicon substrate using precursors (a) HMDSO and (b) HMDSN.

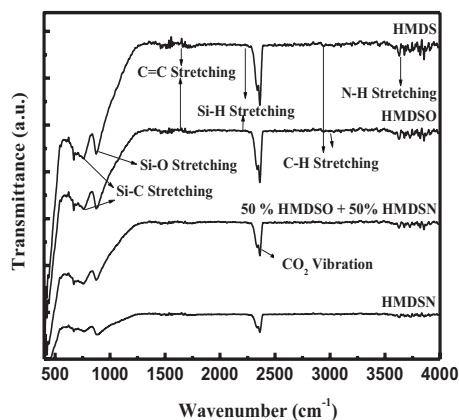


FIG. 3. FTIR spectra of different DLN samples deposited at same rf bias (600 V).

is at 660–680 cm^{-1} , probably due to the symmetric stretching of SiC_2 . The asymmetric Si—C stretching and rocking of CH_3 group in the region 750–800 cm^{-1} are due to Si— $(\text{CH}_3)_3$ vibrations. The strong Si—O stretching band is observed in the region 850–1000 cm^{-1} . A very weak C=C stretching peak appears at 1560 cm^{-1} , which indicates non-graphite bonding of carbon.²³ The Si—H stretching vibration appears at 2200 cm^{-1} . This stretching vibration suggests that silicon is surrounded by some organic environment rather than being incorporated in a silicon oxide network.^{24,25} In FTIR spectra, the C—O₂ vibration appears due to atmospheric carbon (present during the experiment). Some of absorption bands are found in 3100–3700 cm^{-1} region. They represent the stretching of N—H₂, N—H, and O—H bonds. These types of vibrations occur due to presence of nitrogen in the precursors. From Fig. 3, we observe that the wavenumbers are also shifted which may signify the increase in nitrogen content within the films. The C—H stretching is the most important vibration in DLN films, which appears in 2850–3100 cm^{-1} region. The FTIR spectra of different DLN films which appear in 2850–3100 cm^{-1} region are shown in Fig. 4. This absorption spectrum is mainly due to

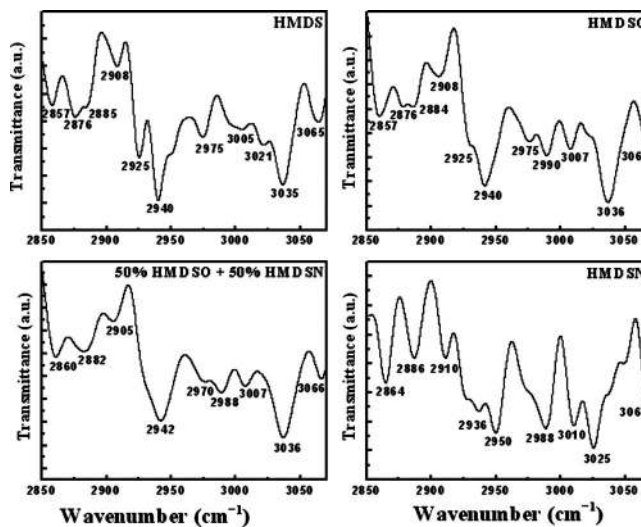


FIG. 4. FTIR spectra of different DLN samples deposited at same rf bias (600 V) in the wave number range 2850–3100 cm^{-1} .

TABLE II. Different types of bonds and corresponding wave numbers of DLN films using FTIR spectroscopy.

Bond type	Wave numbers (cm ⁻¹)
sp^3 C—H ₂	2855–65
sp^3 C—H ₃	2875–85
sp^3 C—H ₂ / sp^3 C—H	2905–25
sp^2 C—H ₂	2940–50
sp^3 C—H ₃	2970–75
sp^2 C—H	3005–10
sp^2 C—H ₂	3020–35
sp^2 C—H	3060–65

the C—H₂ (symmetric and asymmetric) and C—H₃ (symmetric, asymmetric) stretching bands. From C—H stretching vibrations, we can estimate the amount of sp^2 - and sp^3 -hybridized carbon. The different types of sp^2 - and sp^3 -hybridized bonds with corresponding wave numbers in 2850–3100 cm⁻¹ region are shown in Table II. Basically, 2855–2865 cm⁻¹ and 2875–2885 cm⁻¹ represent symmetrical C—H stretching, where as 2905–2925 cm⁻¹ and 2970–2975 cm⁻¹ represent asymmetrical C—H stretching. On the other hand, C—H stretching at 3005–3065 cm⁻¹ shows a graphite bond of planner geometry.¹⁸ In Fig. 4, the band at 2940–2950 cm⁻¹ is suggested due to C—H₂ symmetrical stretching and 3025–3035 cm⁻¹ is suggested due to C—H₂ asymmetrical stretching. The C—H and Si—O stretching vibrations are mainly comprised of the a-C:H and a-Si:O networks.

Raman spectroscopy is one of the most standard techniques to investigate the state of carbon in greater details, because of its sensitivity to the changes in translation symmetry. DLN films are the characteristics of amorphous carbon phase, much like DLC films, which are probably dominated by sp^3 bonding.²⁶ The first order Raman spectra of DLN films is shown in Fig. 5(a) which is usually deconvoluted into Gaussian D and G bands (here D stands for disorder graphite band and G stands for single crystal graphite band). Two broad peaks (D and G) are assigned in the Raman spectra of the DLN films, which are appeared in the wave number region 1000–1800 cm⁻¹, are the typical characteristics of amorphous carbon films. The shape of the spectra varies with substrate material composition. The positions and widths of D and G peaks can be correlated with the films properties (e.g., hardness, wear, and electrical properties) like conventional DLC films.²⁷ The position of the D and G peaks are shifted due to variation in structure of DLN films using different precursors. Figure 5(b) is the Gaussian deconvoluted Raman spectrum of the D and G peaks for DLN films based on HMDS precursor. The D band around 1330 cm⁻¹ corresponds to breathing mode of sp^2 hybridized carbon atoms in hexagonal ring formed by graphite structure. It is the disorder of bond angle, resulting due to disappearance of the long range translation symmetry of polycrystalline graphite and amorphous carbon films. On the other hand, the G band around 1535 cm⁻¹ is related to C—C stretching vibration of sp^2 hybridized carbon atoms in both the rings and chains of graphite layer for single crystalline graphite

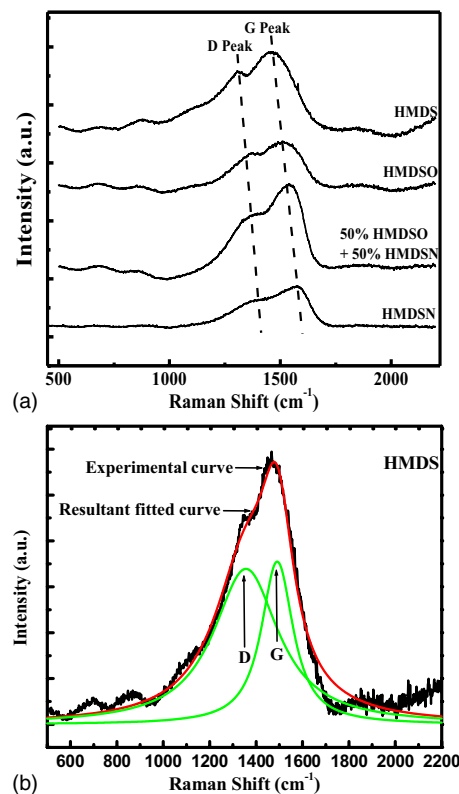


FIG. 5. (Color online) Raman spectra of DLN films deposited at same rf bias (600 V): (a) D and G peaks of different DLN samples (dashed-lines indicate the shift in the peaks) and (b) Gaussian deconvoluted Raman spectra of DLN films (using HMDS precursor) by nonlinear curve fitting method.

structure.^{28–32} In diamond-like films, the intensity and position of D and G peaks are generally related with the ratio of $sp^3:sp^2$ which determines the mechanical and electronic properties of the films. Both the wave number and bandwidth (FWHM) of G band as well as intensity ratio of the D and G peaks (i.e., I_D/I_G) are sometimes used as “graphitization indices” with the objective to relate features of the Raman spectrum to the structure of carbon materials. The peak positions and intensity ratio (I_D/I_G) control the physical properties of the DLN films. Table III shows the peak positions (ω), FWHM (Γ), and intensity ratio (I_D/I_G) of the deconvoluted Gaussian D and G peaks, for different DLN samples.

In XPS, photoelectron survey scan was performed for the binding energy from 0–1000 eV. This study reflects the presence of the different compositions into the surface of the films. Figure 6(a) shows the survey scan of typical DLN films (using HMDSN precursor) grown at rf bias of 600 V. From this figure, it is confirmed that besides carbon (C 1s), silicon (Si 2s, Si 2p), oxygen (O 1s), a small amount of nitrogen (N) is found on the surface of the DLN films. This nitrogen affects the hardness and surface roughness of the films. We have also observed that the DLN films with HMDSN precursor has much more nitrogen content than the other films mentioned above. The Si-, C-, N-, and O-spectra of all DLN films are observed in the binding energy range around 102.3–102.85 eV, 284.32–284.63 eV, 398.3–401.9 eV, and 531.71–531.9 eV, respectively [see Fig. 6(a)]. The fitted C- and Si-spectra using Gaussian profile is shown in Figs. 6(b) and 6(c), respectively. The peaks of C and Si at

TABLE III. Gaussian analysis of Raman spectra of DLN films by nonlinear curve fitting method (where ω : peak position, Γ : FWHM, and I: integrated intensity).

Sample number and precursors	ω_D (cm^{-1})	Γ_D (cm^{-1})	ω_G (cm^{-1})	Γ_G (cm^{-1})	I_D/I_G
(a) HMDS	1357	330	1492	164	1.55
(b) HMDSO	1366	264	1544	134	1.78
(c) 50% HMDSO+50% HMDSN	1378	281	1546	123	1.82
(d) HMDSN	1391	229	1571	117	1.92

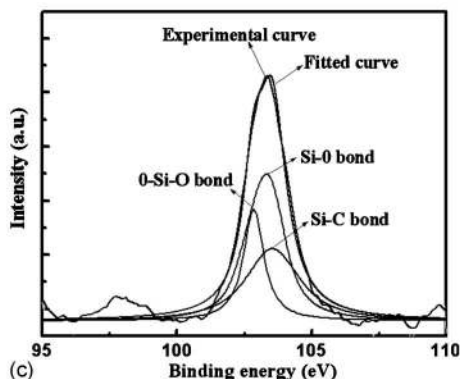
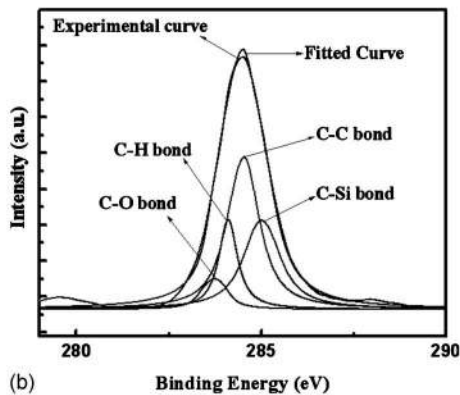
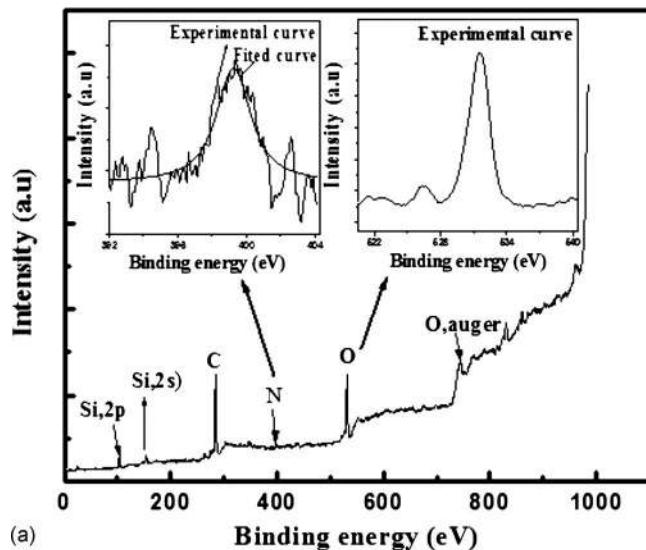


FIG. 6. XPS spectra of DLN films (using HMDSN precursor): (a) The survey scan of DLN films, showing C 1s, O 1s, Si (2s, 2p), and N peaks. (b) Fitted C 1s-spectra with different bonds and (c) Fitted Si-spectra with different bonds.

oms are deconvoluted into several bonding state by using Gaussian deconvolution fitting method (where the distance between peaks, doublets, and width of the individual peaks remain constant during the fitting).^{33,34} In Fig. 6(b), contributions due to C—C, C—H, C—Si, and C—O bonds are observed. On the other hand, the contributions due to Si—C and Si—O bonds are observed in Fig. 6(c). The presence of C—H and Si—O bonds mainly assure the existence of the two interpenetrating networks like a-C:H and a-Si:O, which indirectly proves the structure of DLN films. Also, the C-spectra can be fitted with three peaks correspond to sp^3 -hybridized carbon (diamond), sp^2 hybridized carbon (graphite), and CO (adsorbed gas). A small amount of CO is found in all samples and it may be due to chemisorbed oxygen present into the DLN films during deposition. This phenomenon is also proved by FTIR analysis.

The surface morphologies of DLN films are analyzed by using AFM. Figure 7 shows the AFM image of DLN films (for HMDSN precursor) in two dimensional (2D) and three dimensional (3D) views. From AFM analysis, we have estimated the mean surface roughness (R_a) and maximum peak-to-valley height (R_{max}) of the DLN films, which are 0.292–3.2 nm and 6.1–33 nm, respectively. From this analysis, it is also confirmed that all the DLN films have no surface defects (such as macroparticles and pinholes). Again, very less surface roughness influences the mechanical and tribological performances of the films for microscale and nanoscale devices. Hence, DLN films will provide the better performance for the applications in microelectromechanical systems (MEMS) or nanoelectromechanical systems (NEMS) devices compared to DLC films.³⁵

B. Mechanical properties of DLN films

1. Hardness and elastic modulus

The method of measuring hardness and elastic modulus of thin films by nanoindentation technique is explained by Oliver and Pharr.^{21,36} This method is widely adopted to characterize the mechanical behavior of low dimensional materials, while the numerous refinements have been made to further improvement of its accuracy. The curves (for four different DLN samples) of loading and unloading forces versus displacement into the films, at maximum load up to 20 mN are shown in Fig. 8. This figure shows a good reproducibility of the Nanoindentation test.³⁷ The average hardness of the DLN films is measured using three indents with 20 mN load which is around 9.5–13 GPa. The average reduced elastic modulus of the DLN films is measured under the 20 mN loading force with 300 nm displacement which is around

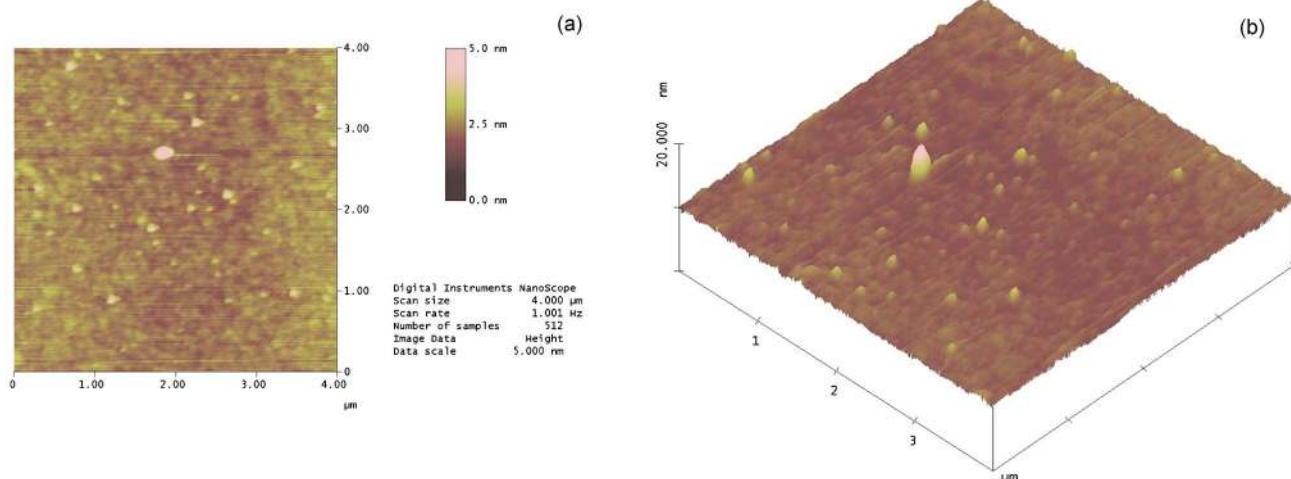


FIG. 7. (Color online) Surface morphology of DLN films (for HMDSN precursor) deposited on silicon substrate: (a) 2D view and (b) 3D view.

90–115 GPa. The reduced elastic modulus (E_r) of the DLN films can be estimated by nanoindentation technique using the following equation:

$$E_r = \frac{\sqrt{\pi} S}{2 \sqrt{A}}, \tag{1}$$

where S is the stiffness of the specimen and A is the projected contact area of the indentation. The elastic modulus (E) of the test material can be found out from

$$\frac{1}{E_r} = \frac{1 - \nu^2}{E} + \frac{1 - \nu_i^2}{E_i}, \tag{2}$$

where E and ν are the elastic modulus and Poisson’s ratio for the tested films, respectively. On the other hand, E_i and ν_i are the same for indenter. The DLN films exhibit elastic modulus

of the order of 90–115 GPa, using $\nu=0.2$, $E_i=1141$ GPa, and $\nu_i=0.07$ under load=20 mN. Figures 9 and 10 show the variation in hardness and modulus of elasticity corresponding to penetration depth. We observe that the hardness of the films increases with increase in penetration depth into the surface (see Fig. 9) and on the other hand, the modulus of elasticity decreases with increase in penetration depth. Moreover, from Raman analysis, it is generally regarded that the higher graphitic fraction in the films provides lower mechanical properties. Hence, the higher value of I_D/I_G ratio provides lower value of hardness of the films. However, the intensity ratio (I_D/I_G) and the frequency of G band for DLN films using HMDS precursor are found to be less compared to other DLN films (see Table III). Hence, the mechanical properties for this type of DLN films are better than the other films. Using nanoindentation test, we observe that the hardness for the above sample is always higher and again the hardness for sample using HMDSN precursor is always lower compared to other samples (see Fig. 9). Further, the elastic modulus decreases with the decrease in hardness of the different films (see Figs. 9 and 10). From FTIR analysis (Fig. 3), we observe the N—H stretching band at 3450 cm^{-1} for DLN films using HMDSN precursor, which suggests that the hardness decreases with N—H bonding effect. At this point, we also mention that the wear resistance decreases with increase in the hardness of films.^{38,39}

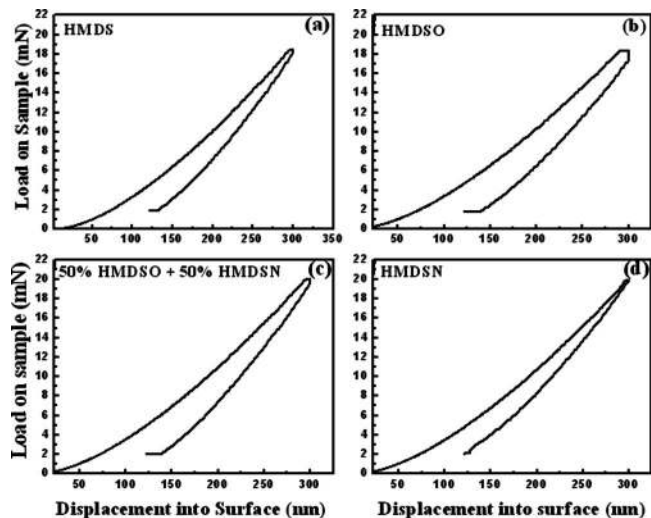


FIG. 8. Loading and unloading curves by Nanoindentation test for DLN films using precursors: (a) HMDS, (b) HMDSO, (c) 50% HMDSO + 50% HMDSN, and (d) HMDSN.

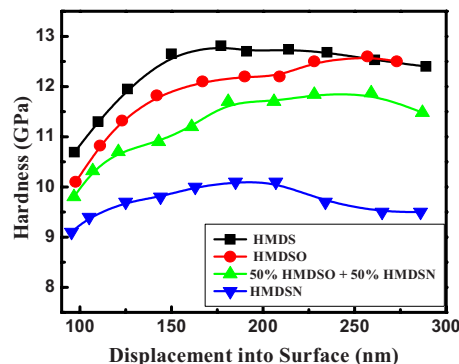


FIG. 9. (Color online) Plots of hardness vs penetration depth for different DLN samples as obtained by nanoindentation test.

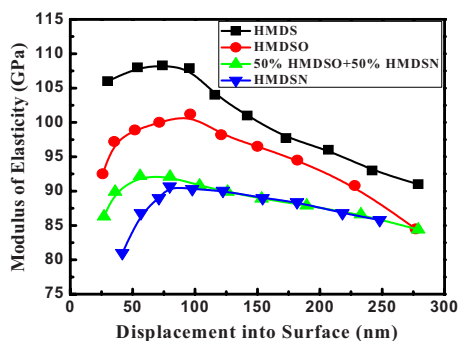


FIG. 10. (Color online) Plots of modulus of elasticity vs penetration depth for different DLN samples as obtained by nanoindentation test.

2. Tribological properties of DLN films

To measure the friction coefficient of the DLN films by scratch test method, the loading rate was 16 N for both normal force and tractional force and the scratch length was about 3 mm. We have estimated the friction coefficient of the samples by taking the ratio of normal force and lateral force. The variation in normal load and tractional force with respect to stroke length, and the corresponding variation in coefficient of friction against normal load, for two different types of DLN films (i.e., films with HMDS and HMDSN precursors) are shown in Fig. 11. The average friction coefficient of DLN films using conical diamond tip is estimated which is nearly 0.03–0.05.

The tribological properties of DLN films are most important for their use as protective coatings. Recently, the DLC films have been used as rigid disk or microelectromechanical or nanoelectromechanical devices. These protective coatings must have excellent wear and tear resistance, high adhesiveness and very low friction coefficient. For DLC

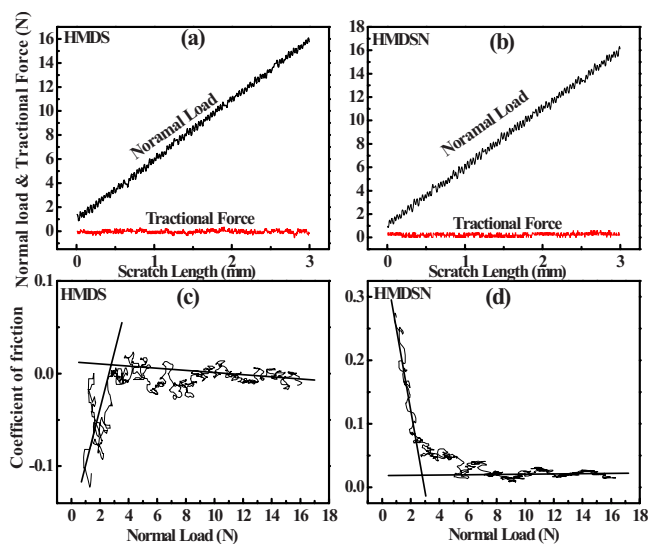


FIG. 11. (Color online) Variation in normal load and tractional force with scratch length for DLN samples prepared using (a) HMDS and (b) HMDSN precursors, respectively. The corresponding variation in friction coefficient with normal load for DLN samples prepared using (c) HMDS and (d) HMDSN precursors, respectively.

films, the friction coefficient is around 1 but for DLN films, friction coefficient is around 0.03–0.05 (as stated above). Hence, for modern microsystems or nanosystems (i.e., MEMS or NEMS), we can use the DLN films compared to DLC films.

IV. DISCUSSION

The diversified structure of DLN thin films, deposited on pyrex glass or silicon substrate using different gas precursors such as HMDS, HMDSO, HMDSN, or their different combinations are achieved by using PECVD technique. The most of our conclusions are drawn from FTIR, Raman spectroscopy, and XPS analysis (a complementary investigation technique). From HRTEM analysis, we have observed that the nanoparticles (like Si_3N_4 , SiC, or SiO_x) are embedded in amorphous matrices of DLN films. The sizes of the nanoparticles (might be silicon nitride, Si_3N_4) on the DLN films deposited using HMDSN precursor were between 6–30 nm. The molecular formula of HMDS, HMDSO, and HMDSN gas precursors are $(\text{CH}_3)_3\text{—Si—Si—}(\text{CH}_3)_3$, $(\text{CH}_3)_3\text{—Si—O—Si—}(\text{CH}_3)_3$, and $(\text{CH}_3)_3\text{—Si—NH—Si—}(\text{CH}_3)_3$, respectively.¹²

These gas precursors consist of Si—Si, Si—C, Si—O, N—H, C—H, and Si—N bonds. Actually, these bonds are broken due to electron temperature of rf power ($\sim 2 \times 10^3 \text{ W m}^{-2}$) inside the PECVD chamber. Therefore, the bonds are broken during films growth, and after multiple gas phase collisions the silicon containing nanoparticles like Si_3N_4 , SiC, and SiO_x were likely formed due to the higher bond-strength of Si—C, Si—N, and Si—O bonds than other existing bonds. We have confirmed the presence of different bondings, such as Si—O, Si—H, Si—C, N—H, C=C, C—H etc in the DLN films using FTIR spectroscopy. The low compressive stress of the DLN films may be due to the incorporation of the nanoparticles into a-C:H and a-Si:O networks.¹⁰

In amorphous carbon structure, there is a possibility to form both threefold coordinate (sp^2 -site) as in graphite and fourfold coordinate (sp^3 -site) as in diamond.⁴⁰ Each of the four valance electron lies in the sp^3 -site forms σ -bonds with neighbors.⁴¹ In sp^2 -site, only three electrons are used in σ -bonds and the fourth electron forms a π -bond, which lies normal to the σ -bonding plane. In sp^2 -site, only the π -bond is weakly bonded, and hence, it usually lies closest to the Fermi level and controls the electronic properties of the films. On the other hand, in sp^3 -site, the σ -bond controls the mechanical properties of the films.⁴² These mechanical and electrical properties are very important parameters for every material. From the Raman spectroscopy of the DLN films, the D and G bands shifted toward the lower wave numbers, as compared to the conventional DLC films. As pointed out by Tamor and Vassell,⁴⁰ the increase in the concentration of sp^3 carbon in the films, induces the shift in the G band to the lower wave numbers. Once more, Beeman *et al.*⁴³ observed that due to increase in sp^3 bonded atomic sites in amorphous carbon results a shift in the G band to a lower frequency. Richter *et al.*⁴⁴ suggested that the frequency shift in the G band is caused due to the alteration of the force constant

associated with variation in the sp^3 bonded fraction. Therefore, following our Raman spectroscopic results [see Fig. 5(a)], the DLN films should have higher concentrations of sp^3 carbon than the conventional DLC films. Again, the shift in G band of the films to a higher frequency indicates a decrease in the ratio $sp^3:sp^2$. Also it was reported that if graphitic contents of the films increases, the I_D/I_G ratio increases, which indicates the phase transformation of disordered diamond-like structure to ordered graphitic structure.^{45,46}

The XPS analysis has confirmed the presence of C—H, C—O, C—Si, Si—O, C—C bonds and nitrogen (N) in the DLN films. The nitrogen impurity exists into the DLN films in the form of (sp^2) C—N bond. Due to presence of nitrogen in the DLN films, both the hardness and surface roughness decreases. Hence, due to nitrogen impurity in the DLN films, the surface morphology is improved but the quality of diamond films is reduced (for low hardness).

V. CONCLUSIONS

DLN films have been deposited on glass (pyrex) or silicon substrate using HMDS, HMDSO, HMDSN, or their mixture as a gas precursor by PECVD technique. From GIXRD, FTIR, Raman spectroscopy, and XPS analysis, we conclude that the hydrocarbon groups are bonded with two interpenetrating networks (a-C:H and a-Si:O) of DLN films. And also from HRTEM analysis, DLN films contain Si_3N_4 , SiC, and SiO_x nanoparticles within amorphous matrix, which help to reduce the compressive stress of the films. Raman spectroscopy shows that the DLN films should have higher concentrations of sp^3 carbon than the conventional DLC films. High sp^3 contents influence the mechanical properties of the films. The I_D/I_G ratio increases due to increase in nitrogen contents into the films (e.g., DLN films produced by HMDSN), and as a result, hardness and elastic modulus are decreased. Therefore, we can conclude that HMDS, HMDSO precursors are better than HMDSN precursor for the formation of DLN films. The measured hardness and elastic modulus of the DLN samples are around 9.5–13 GPa and 90–115 GPa, respectively. The surface roughness (R_a) and maximum peak to valley height (R_{max}) of these DLN films are 0.292–3.2 nm and 6.1–33 nm, respectively. The friction coefficient of DLN samples are around 0.03–0.05. Finally, we conclude that the DLN films have an excellent potential for industrial applications compared to DLC films. DLN films with high hardness, high elastic modulus, low friction coefficient, low surface roughness and low compressive stresses, are highly suitable for the coating materials in MEMS or NEMS devices.

ACKNOWLEDGMENTS

The authors (T. S. Santra, P. Patel, and T. K. Barik) gratefully acknowledge the kind cooperation of Dr. Jagannath, BARC, Mumbai for his help in XPS measurement, and also Dr. A. S. Bhattacharyya, NML, Jamshedpur for his cooperation in Nanoindentation and Scratch test. We would

also like to express our heartfelt gratitude to Prof. S. K. Ray, Dr. A. Dhar, Dr. B. Mishra, and Mr. S. Sarkar of IIT, Kharagpur for their help in arranging AFM, GIXRD, Raman spectroscopic measurements, and writing the article, respectively.

- ¹M. M. Morshed, B. P. McNamara, D. C. Cameron, and M. S. J. Hashmi, *Surf. Coat. Technol.* **163–164**, 541 (2003).
- ²S. R. P. Silva, J. Robertson, W. I. Milne, and G. A. J. Amaratunga, *Amorphous Carbon: State of the Art* (World Scientific, Singapore, 1988).
- ³Y. Lifshitz, *Diamond Relat. Mater.* **8**, 1659 (1999).
- ⁴B. Bhushan, *Diamond Relat. Mater.* **8**, 1985 (1999).
- ⁵W. Tillmann, E. Vogli, and F. Hoffmann, *Thin Solid Films* **516**, 262 (2007).
- ⁶A. Shirakura M. Nakaya, Y. Koga, H. Kodama, T. Hasebe, and T. Suzuki, *Thin Solid Films* **494**, 84 (2006).
- ⁷D. Liu, G. Benstetter, and E. Lodermeier, *Thin Solid Films* **436**, 244 (2003).
- ⁸M. P. Siegal, J. C. Barbour, P. N. Provencia, D. R. Tallant, and T. A. Friedmann, *Appl. Phys. Lett.* **73**, 759 (1998).
- ⁹M. P. Siegal, D. R. Tallant, P. N. Provencia, D. L. Overmyer, R. L. Simpson, and L. J. Martinez-Miranda, *Appl. Phys. Lett.* **76**, 3052 (2000).
- ¹⁰T. Sharda, T. Soga, T. Jimbo, and M. Umeno, *Appl. Phys. Lett.* **80**, 2880 (2002).
- ¹¹G. Cicala, P. Capezzuto, G. Bruno, L. Schiavulli, and G. Amato, *J. Appl. Phys.* **79**, 8856 (1996).
- ¹²L. Y. Chen and F. C. N. Hong, *Appl. Phys. Lett.* **82**, 3526 (2003).
- ¹³S. W. Rynders, A. Schleele, and P. W. Bohn, *J. Appl. Phys.* **69**, 2951 (1991).
- ¹⁴C. Venkatraman, D. J. Kester, A. Goel, and D. J. Bray, *The Minerals, Metals and Materials Society, International Conference on Surface Modification Technologies IX* (ASM-TMS, Cleveland, OH, 1995), Vol. 21.
- ¹⁵C. A. Davis, *Thin Solid Films* **30**, 226 (1993).
- ¹⁶J. Robertson, *Diamond Relat. Mater.* **2**, 984 (1993).
- ¹⁷T. Das, D. Ghosh, T. K. Bhattacharya, and T. Maiti, *J. Mater. Sci.: Mater. Med.* **18**, 493 (2007).
- ¹⁸V. Palshin, E. I. Meletis, S. Ves, and S. Logothetidis, *Thin Solid Films* **270**, 165 (1995).
- ¹⁹V. F. Dorfman and B. N. Pypkin, *Surf. Coat. Technol.* **48**, 193 (1991).
- ²⁰V. F. Dorfman and B. N. Pypkin, U.S. Patent No. 5,352,493 (1994).
- ²¹W. C. Oliver and G. M. Pharr, *J. Mater. Res.* **7**, 1564 (1992).
- ²²D. A. Skoog, F. J. Holler, and T. A. Nieman, *Principles of Instrumental Analysis*, 4th ed. (Harcourt Brace & Co., Philadelphia, 1998), Chap. 16.
- ²³M. P. Nadler, T. M. Donovan, and A. K. Green, *Thin Solid Films* **116**, 241 (1984).
- ²⁴N. Mutsukura and K. Akita, *Thin Solid Films* **349**, 115 (1999).
- ²⁵A. Ungureanu, O. D. Trong, E. Dumitriu, and S. Kaliaguine, *Appl. Catal., A* **254**, 203 (2003).
- ²⁶D. R. Tallant, J. E. Parmeter, M. P. Siegal, and R. L. Simpson, *Diamond Relat. Mater.* **4**, 191 (1995).
- ²⁷B. Marchon, N. Heiman, M. R. Khan, A. Lautie, W. J. Ager, and D. K. Veris, *J. Appl. Phys.* **69**, 5748 (1991).
- ²⁸F. Tuinstra and J. L. Koenig, *J. Chem. Phys.* **53**, 1126 (1970).
- ²⁹R. O. Dillon and J. A. Woollam, *Phys. Rev. B* **29**, 3482 (1984).
- ³⁰W. J. Yang, Y. H. Choa, T. Sekino, K. B. Shim, K. Niihara, and K. H. Auh, *Mater. Lett.* **57**, 3305 (2003).
- ³¹J. Wu, C. Chen, C. Shin, M. Li, M. Leu, and A. Li, *Thin Solid Films* **517**, 1141 (2008).
- ³²R. Gago, M. Vinnichenko, H. U. Jager, A. U. Belov, I. Jimenez, N. Huang, H. Sun, and M. F. Maitz, *Phys. Rev. B* **72**, 014120 (2005).
- ³³S. Contarini, E. Lambers, and P. H. Holloway, *Appl. Surf. Sci.* **62**, 181 (1992).
- ³⁴F. Verpoort, A. R. Bossuyt, and L. Verdonck, *J. Electron Spectrosc. Relat. Phenom.* **82**, 151 (1996).
- ³⁵J. K. Luo, Y. Q. Fu, H. R. Le, J. A. Williams, S. M. Spearing, and W. I. Milne, *J. Micromech. Microeng.* **17**, S147 (2007).
- ³⁶W. C. Oliver and G. M. Pharr, *J. Mater. Res.* **19**, 3 (2004).
- ³⁷N. Savvides and T. J. Bell, *J. Appl. Phys.* **72**, 2791 (1992).
- ³⁸*Coatings Tribology—Properties, Techniques and Applications in Surface Engineering*, edited by K. Holmberg, A. Matthews, and D. Dowson (Elsevier, Amsterdam, 1994), p. 93.
- ³⁹E. Dekempeneer, K. V. Acker, K. Vercammen, J. Meneve, D. Neerincx, S. Eufinger, W. Pappaert, M. Sercu, and J. Smeets, *Surf. Coat. Technol.* **142–144**, 669 (2001).

- ⁴⁰M. A. Tamor and W. C. Vassell, *J. Appl. Phys.* **76**, 3823 (1994).
- ⁴¹J. Robertson, *Adv. Phys.* **32**, 361 (1983).
- ⁴²J. Robertson, *Pure Appl. Chem.* **66**, 1789 (1994).
- ⁴³D. Beeman, J. Silverman, R. Lynds, and M. R. Anderson, *Phys. Rev. B* **30**, 870 (1984).
- ⁴⁴A. Richter, H. J. Scheibe, W. Pompe, K. W. Brezeinka, and I. Muhling, *J. Non-Cryst. Solids* **88**, 131 (1986).
- ⁴⁵F. L. Feire, C. A. Achete, G. Mariotto, and R. Centeri, *J. Vac. Sci. Technol. A* **12**, 3048 (1994).
- ⁴⁶W. J. Meng and B. A. Gillispie, *J. Appl. Phys.* **84**, 4314 (1998).